2010

Efficient Tether Dynamic Model Formulation Using Recursive Rigid-Body Dynamics

Brad Hembree
University of Alabama - Huntsville

Nathan Slegers
George Fox University, nslegers@georgefox.edu

Efficient tether dynamic model formulation using recursive rigid-body dynamics

B Hembree and **N Slegers***
Department of Mechanical and Aerospace Engineering, University of Alabama in Huntsville, Huntsville, Alabama, USA

Abstract: A computationally efficient discrete model for low-strain tethers used in many engineering applications is developed without the use of elastic elements. The tether is modelled using N links, with each link treated as a body of revolution where it is assumed the tether spin is negligible to the dynamics, resulting in each link having only two degrees of freedom. A recursive algorithm is developed for the dynamic equations, with the solution procedure being an order N method requiring only a 2×2 matrix inversion, resulting in approximately half the computations of the general recursive algorithm. A comparison between the proposed efficient recursive rigid-body model and a lumped point mass model shows that the absence of stiff elastic elements eliminates high-frequency axial vibrations that appear in many lumped point mass tether models. The absence of high-frequency axial vibration facilitates numerical integration of the equations, providing further improvement in computational speed.

Keywords: tether dynamics, recursive dynamics, joint-coordinate, Newtonian dynamics

1 INTRODUCTION

Dynamic modelling of bodies connected by cables, chains, and tethers is common to many engineering disciplines. Some examples are tethered balloons [**1**], a fly rod and line [**2, 3**], cables towed by aircraft [**4**] and under water [**5**], excavators [**6**], and tethered munitions [**7**]. The previous models listed all have some similarities. A primary body (ground, aircraft, ship, and projectile) and an end body or bodies (balloon, payload, and bucket) connected by a continuous cable, chain, or tether. While the cable, chain, or tether is continuous, it is modelled using discrete elements. The simplest models use lumped mass bodies connected with elastic elements [**4, 7**] where each mass has only three degrees of freedom (DOFs) and the simple elastic elements allow accelerations to be easily found. The addition of a visco-elastic element in reference [**6**] improves the performance of the lumped mass model for stiff tethers while also adding an extra state for each visco-elastic element. Regardless of which element is used, elastic or visco-elastic, the lumped mass models are appealing, because they result in extremely simple, computationally efficient models even for large numbers of elements. Model complexity is further increased in reference [**1**] where beam elements are used rather than lumped masses. Using beam elements allows modelling of bending moments but requires a finite-element non-linear solver so that the computational burden is much higher than the lumped mass models. A similar approach was used to model a fly rod and line [**2, 3**] using a flexible beam model with two modes to model the fly rod while a continuum model and finite-difference method was used to model a tapered fly line. For complex multibody problems with both rigid and flexible bodies, such as rotorcraft blade–hub configurations, formulations using finite-element methods have also been proposed [**8, 9**].

For a class of systems, the tether is sufficiently strong and/or the loads from the attached mass are sufficiently small so that the strain can be considered negligible. Examples include lighter than air systems where the tension from buoyancy is small as in reference [**1**] and an excavator [**6**] where connecting chains are not flexible. In these cases, the lumped mass model with elastic elements is only a mathematical convenience. In addition, when tether strain is small, individual

* *Corresponding author: Department of Mechanical and Aerospace Engineering, University of Alabama in Huntsville, Technology Hall, Huntsville, Alabama 35899, USA.*
email: slegers@mae.uah.edu

elastic elements must be made extremely stiff in order to make the static stiffness representative of the actual tether. Using many extremely stiff elastic elements, results in the potential for the appearance of numerical integration problems and high-frequency axial dynamics not present in the physical system. This article models tethers with negligible strain using a chain of links connected by spherical joints, rather than using stiff elastic elements and lumped masses. The resulting model takes the form of an open chain common to multi-body dynamics. An additional advantage of using a chain of links rather than point masses connected by elastic elements is the ability to include bending stiffness and transverse damping into the model. This is particularly important in cases where the fluid density and speed is low [**1**, **6**] such that internal friction and structural damping are not dominated by drag forces.

Computational multi-body dynamics has seen continued development in solution methods and analysis. An overview of advancements in computer simulations of multi-body dynamics is provided by Orlandea [**10**]. Nikravesh [**11**] reviews three formulations of multi-body equations of motion using Newtonian methods. The first two methods called body and point-coordinate formulations by Nikravesh are simple to formulate but result in large numbers of differential-algebraic equations. The third method, joint-coordinate formulation, results in a smaller set of differential equations without constraints. This article takes an approach similar to the joint-coordinate method where each link's dynamics are represented by a relative joint velocity, resulting in a set of unconstrained differential equations representing the tether.

The unconstrained set of differential equations can be solved using either an order N^3 method by inverting a system mass matrix [**12**, **13**] or by recursive rigid-body dynamics which is order N [**14**]. As the number of bodies N increases, the order N method is more computationally efficient [**15**]. As shown by Tong [**16**], the recursive rigid-body formulation for general bodies can be simplified by taking advantage of mass properties and kinematic behaviours. Specifically, Tong [**16**] analysed gyroscopic bodies with only a single axis of revolution applicable to reaction wheels on satellites. In this work, each link is treated as a body of revolution and it is assumed that tether spin is negligible to the dynamics. Each link then only has two DOFs and the order N recursive formulation only requires inversion of a 2×2 matrix. The proposed recursive rigid-body tether formulation results in computations on the same order as the three DOFs lumped mass models with an additional state for a visco-elastic element. Furthermore, the elimination of high stiffness springs allows larger integration time steps, further improving computation speeds. The result is a computationally efficient model that can accurately represent a low-strain tether used in many engineering applications without the need to add stiff elastic elements.

2 DEFINITIONS

The tether is divided into a chain of N bodies connected by spherical joints with each link being a body of revolution. Figure 1 shows the tether attached to the ground with the jth body, b_j, having two connections, joints c_{j-1} and c_j, and an external load applied to the Nth body. The Nth body, b_N, is the terminal link, body b_1 is the root link, and b_0 is a fixed body or ground where connection c_0 is stationary. A body, b_j, is attached to its parent, b_{jp}, in the direction of the ground where the subscript jp represents the parent of j. Body b_0 is attached to a fixed or inertial frame (I) defined by three orthogonal unit vectors, $\boldsymbol{i}_I$, $\boldsymbol{j}_I$, and $\boldsymbol{k}_I$. A body reference frame is assigned to each link, as shown in Fig. 2, with the origin at the link's mass centre and the vector $\boldsymbol{i}_j$ collinear to the mass centre and joints on body j with $\boldsymbol{j}_j$ and $\boldsymbol{k}_j$ defined to form an orthogonal triad.

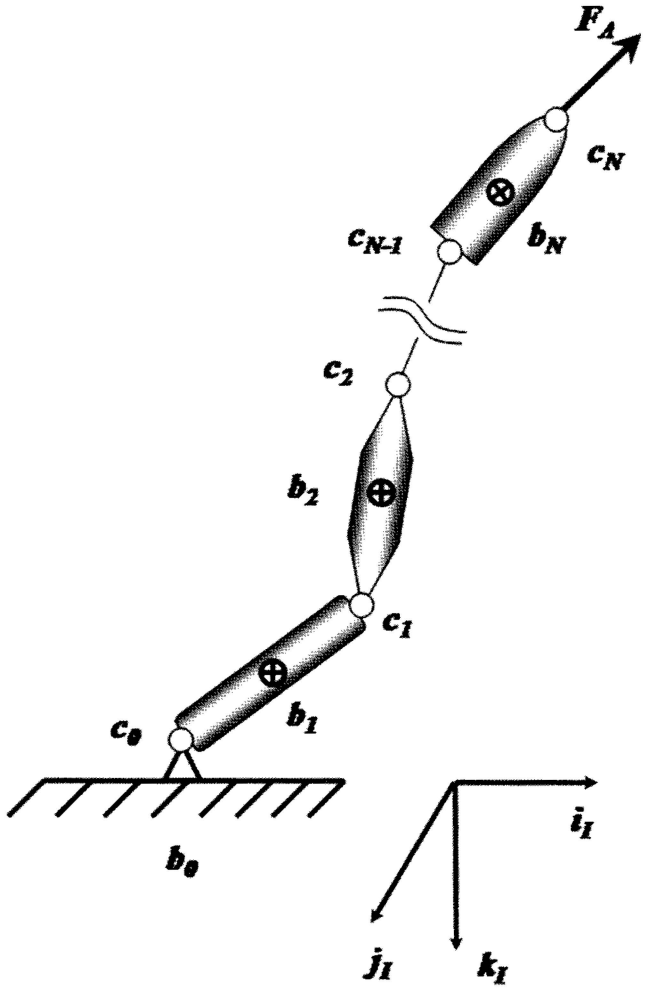

Fig. 1 General tether model for 'N' number of rigid bodies

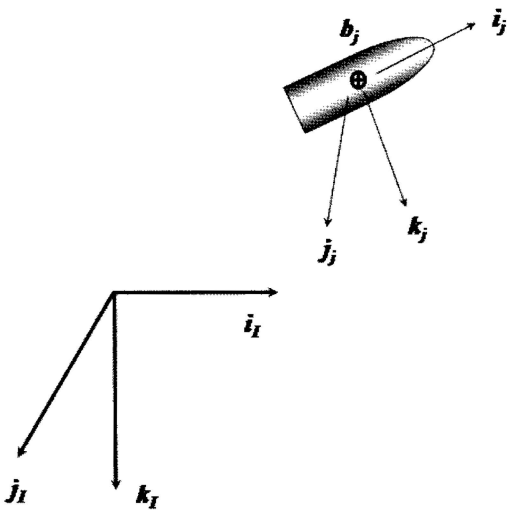

Fig. 2 Moving frame of reference for a general jth body or link

The orientation of the jth body frame is defined by a sequence of three body-fixed rotations. Starting from the inertial frame, the jth body frame is defined by rotations about the $\boldsymbol{k}, \boldsymbol{j}$, and $\boldsymbol{i}$ axes by angles ψ_j, θ_j, and φ_j, respectively. In order to avoid a singularity in the rotation kinematics, the orientation can alternatively be defined by the four quaternion parameters q_{0j}, q_{1j}, q_{2j}, and q_{3j} [17] resulting in the transformation from the inertial frame, I, to the j frame given by

$$\mathbf{T}_I^j = \begin{bmatrix} 2q_{0j}^2 - 1 + 2q_{1j}^2 & 2q_{1j}q_{2j} + 2q_{0j}q_{3j} & 2q_{1j}q_{3j} - 2q_{0j}q_{2j} \\ 2q_{1j}q_{2j} - 2q_{0j}q_{3j} & 2q_{0j}^2 - 1 + 2q_{2j}^2 & 2q_{2j}q_{3j} + 2q_{0j}q_{1j} \\ 2q_{1j}q_{3j} + 2q_{0j}q_{2j} & 2q_{2j}q_{3j} - 2q_{0j}q_{1j} & 2q_{0j}^2 - 1 + 2q_{3j}^2 \end{bmatrix} \tag{1}$$

where

$$\begin{aligned} q_{0j} &= \cos\left(\frac{\psi_j}{2}\right)\cos\left(\frac{\theta_j}{2}\right)\cos\left(\frac{\phi_j}{2}\right) \\ &\quad + \sin\left(\frac{\psi_j}{2}\right)\sin\left(\frac{\theta_j}{2}\right)\sin\left(\frac{\phi_j}{2}\right) \\ q_{1j} &= \cos\left(\frac{\psi_j}{2}\right)\cos\left(\frac{\theta_j}{2}\right)\sin\left(\frac{\phi_j}{2}\right) \\ &\quad - \sin\left(\frac{\psi_j}{2}\right)\sin\left(\frac{\theta_j}{2}\right)\cos\left(\frac{\phi_j}{2}\right) \\ q_{2j} &= \cos\left(\frac{\psi_j}{2}\right)\sin\left(\frac{\theta_j}{2}\right)\cos\left(\frac{\phi_j}{2}\right) \\ &\quad + \sin\left(\frac{\psi_j}{2}\right)\cos\left(\frac{\theta_j}{2}\right)\sin\left(\frac{\phi_j}{2}\right) \\ q_{3j} &= \sin\left(\frac{\psi_j}{2}\right)\cos\left(\frac{\theta_j}{2}\right)\cos\left(\frac{\phi_j}{2}\right) \\ &\quad - \cos\left(\frac{\psi_j}{2}\right)\sin\left(\frac{\theta_j}{2}\right)\sin\left(\frac{\phi_j}{2}\right) \end{aligned} \tag{2}$$

A transformation from the $j-1$ frame to the j frame can be formed using equation (1) and is given as

$$\mathbf{T}_{j-1}^j = \left(\mathbf{T}_j^I\right)^{\mathrm{T}} \mathbf{T}_{j-1}^I \tag{3}$$

Position vectors from the $j-1$ connection to the jth body mass centre are conveniently expressed in the b_j frame as $\boldsymbol{r}_j^{\mathrm{m}} = x_{\mathrm{m}j}\boldsymbol{i}_j$. Similarly, the vector from connection $j-1$ to connection j, also expressed in the b_j frame, is defined as $\boldsymbol{r}_j^{\mathrm{c}} = x_{\mathrm{c}j}\boldsymbol{i}_j$. Both vectors $\boldsymbol{r}_j^{\mathrm{m}}$ and $\boldsymbol{r}_j^{\mathrm{c}}$ have only an $\boldsymbol{i}_j$ component as a result of each body's symmetry.

3 KINEMATICS

The tether configuration in Fig. 1 has spherical joints connecting the N bodies with no applied twisting torque at the ground or terminal link. In addition, the bodies are slender such that the moment of inertia I_{xx} will be small compared to the other moments of inertia. This combination results in spinning dynamics of each body having a minimal affect of the tether's overall motion. Elimination of tether spin will later aid in efficient computation of recursive dynamics. The angular velocity of jth body with respect to the inertial frame of reference is then defined as

$$\boldsymbol{\omega}_{j/I} = q_j\boldsymbol{j}_j + r_j\boldsymbol{k}_j \tag{4}$$

where the spin rate, p_j, is zero. The angular velocity of the jth link, $\boldsymbol{\omega}_{j/I}$, may also be written as the sum of the previous body's angular velocity and the relative angular velocity of the jth link and its preceding link $\boldsymbol{\omega}_{j/j-1}$

$$\boldsymbol{\omega}_{j/I} = \boldsymbol{\omega}_{j/j-1} + \mathbf{T}_{j-1}^j\boldsymbol{\omega}_{j-1/I} \tag{5}$$

with $\boldsymbol{\omega}_{j/j-1}$ expressed in the b_j frame. Equation (5) can equivalently be expressed in component form

$$\boldsymbol{\omega}_{j/I} = \begin{Bmatrix} \omega_{xj} \\ \omega_{yj} \\ \omega_{zj} \end{Bmatrix} + \mathbf{T}_{j-1}^j \begin{Bmatrix} 0 \\ q_{j-1} \\ r_{j-1} \end{Bmatrix} = \begin{Bmatrix} 0 \\ q_j \\ r_j \end{Bmatrix} \tag{6}$$

where ω_{xj}, ω_{yj}, and ω_{zj} are the components of the relative angular velocity $\boldsymbol{\omega}_{j/j-1}$. Equation (6) can be separated into two parts

$$\omega_{xj} = -\tilde{\mathbf{T}}_{j-1}^j \begin{Bmatrix} q_{j-1} \\ r_{j-1} \end{Bmatrix} \tag{7}$$

where $\tilde{\mathbf{T}}_{j-1}^j$ is a 1×2 submatrix formed from the second and third elements of the first row of $\mathbf{T}_{j-1}^j$, and

$$\tilde{\boldsymbol{\omega}}_{j/I} = \begin{Bmatrix} \omega_{yj} \\ \omega_{zj} \end{Bmatrix} + \hat{\mathbf{T}}_{j-1}^j \begin{Bmatrix} q_{j-1} \\ r_{j-1} \end{Bmatrix} = \begin{Bmatrix} q_j \\ r_j \end{Bmatrix} \tag{8}$$

where $\hat{\mathbf{T}}_{j-1}^j$ is a 2×2 submatrix formed from the second and third columns of the second and third rows of $\mathbf{T}_{j-1}^j$.

Note, the root link b_1 is a special case because for the ground b_0, both q_0 and r_0 are zero, resulting in

$$\omega_{x1} = 0$$
$$\tilde{\boldsymbol{\omega}}_{1/I} = \begin{Bmatrix} \omega_{y1} \\ \omega_{z1} \end{Bmatrix} = \begin{Bmatrix} q_1 \\ r_1 \end{Bmatrix} \tag{9}$$

Differentiation of the angular velocity with respect to the inertial frame results in the angular acceleration of the jth body taking the recursive form

$$\boldsymbol{\alpha}_{j/I} = \dot{\boldsymbol{\omega}}_{j/j-1} + \boldsymbol{\omega}_{j/I} \times \boldsymbol{\omega}_{j/j-1} + \mathbf{T}^j_{j-1}\boldsymbol{\alpha}_{j-1/I} \tag{10}$$

where $\dot{\boldsymbol{\omega}}_{j/j-1}$ is the angular acceleration of b_j with respect to b_{j-1} expressed in the b_j frame. Expansion of equation (10) into matrix form results in

$$\boldsymbol{\alpha}_{j/I} = \begin{Bmatrix} 0 \\ \dot{q}_j \\ \dot{r}_j \end{Bmatrix} = \begin{Bmatrix} \dot{\omega}_{xj} \\ \dot{\omega}_{yj} \\ \dot{\omega}_{zj} \end{Bmatrix} + \begin{Bmatrix} -r_j\omega_{yj} + q_j\omega_{zj} \\ r_j\omega_{xj} \\ -q_j\omega_{xj} \end{Bmatrix} + \mathbf{T}^j_{j-1} \begin{Bmatrix} 0 \\ \dot{q}_{j-1} \\ \dot{r}_{j-1} \end{Bmatrix} \tag{11}$$

The first row of equation (11) is satisfied by equation (7). Substitution of equation (7) into the remaining two equations results in

$$\tilde{\boldsymbol{\alpha}}_{j/I} = \begin{Bmatrix} \dot{q}_j \\ \dot{r}_j \end{Bmatrix} = \begin{Bmatrix} \dot{\omega}_{yj} \\ \dot{\omega}_{zj} \end{Bmatrix} - \begin{Bmatrix} r_j \\ -q_j \end{Bmatrix} \tilde{\mathbf{T}}^j_{j-1} \begin{Bmatrix} q_{j-1} \\ r_{j-1} \end{Bmatrix} + \hat{\mathbf{T}}^j_{j-1} \begin{Bmatrix} \dot{q}_{j-1} \\ \dot{r}_{j-1} \end{Bmatrix} \tag{12}$$

which can be written compactly as

$$\tilde{\boldsymbol{\alpha}}_{j/I} = \dot{\boldsymbol{\omega}}_j + \boldsymbol{\lambda}_j + \hat{\mathbf{T}}^j_{j-1}\tilde{\boldsymbol{\alpha}}_{j-1/I} \tag{13}$$

$$\boldsymbol{\lambda}_j = \begin{Bmatrix} -r_j \\ q_j \end{Bmatrix} \tilde{\mathbf{T}}^j_{j-1} \begin{Bmatrix} q_{j-1} \\ r_{j-1} \end{Bmatrix} \tag{14}$$

where $\dot{\boldsymbol{\omega}}_j = \begin{Bmatrix} \dot{\omega}_{yj} & \dot{\omega}_{zj} \end{Bmatrix}^{\mathrm{T}}$

Acceleration of the jth body's mass centre, $\boldsymbol{a}^{\mathrm{m}}_j$, and connection joint j's acceleration, $\boldsymbol{a}^{\mathrm{c}}_j$ for $j = 0 - (N-1)$, can be written in the b_j frame as

$$\boldsymbol{a}^{\mathrm{m}}_j = \mathbf{T}^j_{j-1}\boldsymbol{a}^{\mathrm{c}}_{j-1} + \boldsymbol{\alpha}_{j/I} \times \boldsymbol{r}^{\mathrm{m}}_j + \boldsymbol{\omega}_{j/I} \times \boldsymbol{\omega}_{j/I} \times \boldsymbol{r}^{\mathrm{m}}_j \tag{15}$$

$$\boldsymbol{a}^{\mathrm{c}}_j = \mathbf{T}^j_{j-1}\boldsymbol{a}^{\mathrm{c}}_{j-1} - \boldsymbol{r}^{\mathrm{c}}_j \times \boldsymbol{\alpha}_{j/I} + \boldsymbol{\omega}_{j/I} \times \boldsymbol{\omega}_{j/I} \times \boldsymbol{r}^{\mathrm{c}}_j \tag{16}$$

where it is noted that $\boldsymbol{a}^{\mathrm{c}}_0 = 0$ since joint zero is attached to the ground.

The angular acceleration components of b_j (equation (13)) and acceleration of the $j-1$ joint (equation (16)) can be combined into a 5×1 acceleration vector $\dot{\boldsymbol{\nu}}_j = \{\tilde{\boldsymbol{\alpha}}_{j/I}\boldsymbol{a}^{\mathrm{c}}_{j-1}\}^{\mathrm{T}}$ and written

$$\dot{\boldsymbol{\nu}}_j = \mathbf{D}_j\dot{\boldsymbol{\nu}}_{j-1} + \mathbf{G}_j\dot{\boldsymbol{\omega}}_j + \boldsymbol{\Lambda}_j \tag{17}$$

where

$$\mathbf{D}_j = \begin{bmatrix} \hat{\mathbf{T}}^j_{j-1} & 0 \\ (\hat{\mathbf{S}}^{\mathrm{c}}_j)^{\mathrm{T}} & \mathbf{T}^{j-1}_{j-2} \end{bmatrix}, \quad \mathbf{G}_j = \begin{bmatrix} \mathbf{E}_2 \\ 0 \end{bmatrix} \tag{18}$$

$$\boldsymbol{\Lambda}_j = \begin{bmatrix} \boldsymbol{\lambda}_j \\ \boldsymbol{\omega}_{j-1/I} \times \boldsymbol{\omega}_{j-1/I} \times \boldsymbol{r}^{\mathrm{c}}_{j-1} \end{bmatrix}, \quad \hat{\mathbf{S}}^{\mathrm{c}}_j = \begin{bmatrix} 0 & 0 & -x_{cj} \\ 0 & x_{cj} & 0 \end{bmatrix} \tag{19}$$

Note that for $j = 0$, equation (17) reduces to $\dot{\boldsymbol{\nu}}_1 = \mathbf{G}_1\dot{\boldsymbol{\omega}}_1$ because $\dot{\boldsymbol{\nu}}_0 = 0$ and $\boldsymbol{\Lambda}_1 = 0$.

4 RECURSIVE DYNAMIC EQUATIONS

A Newtonian approach is used to form the necessary dynamic equations for the tether model. A total of $2N$ vector equations are assembled where these equations will consist of N force equations and N moment equations. In order to begin forming these equations, the forces and moments acting on terminal and non-terminal bodies are shown in Figs 3 and 4, respectively. Each body has weight, $\boldsymbol{W}_j$, and an external force, $\boldsymbol{F}_{\mathrm{D}j}$, associated with it, both defined in the inertial frame. A reaction force, $-\boldsymbol{R}_j$, on body b_j, defined in the b_j frame, occurs at the jth joint for all j except for the terminal body. An equal, but opposite reaction, $\boldsymbol{R}_j$, is present on body b_{j+1}. Similarly, a moment, $-\boldsymbol{L}_j$, on body b_j, also defined in the b_j frame, occurs at the jth joint for all j except for the terminal body. An equal but opposite moment, $\boldsymbol{L}_j$, is also present on body b_{j+1}. The only

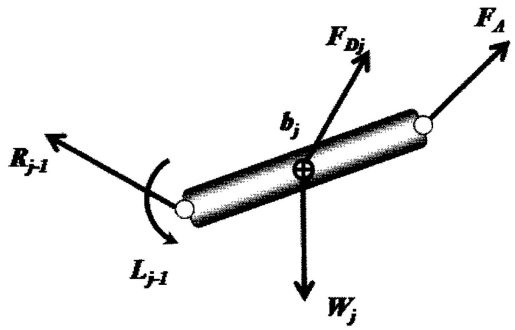

Fig. 3 Terminal body force and moment definitions

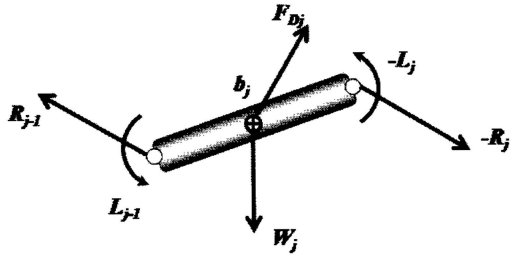

Fig. 4 Non-terminal body force and moment definitions

limitation on $\boldsymbol{L}_j$ is that since the spin dynamics are neglected, the joint cannot impart a twisting moment. Finally, there is an external load, $\boldsymbol{F}_{\mathrm{A}}$, applied to the end of the terminal body.

Dynamic equations are formed by summing forces and moments for individual links with the moment equation expressed in the j body frame and the force equation expressed in the $j-1$ body frame. The two vector equations can be put in a recursive form where moving through the tether from the terminal link towards the root link, equations for the $j-1$ links contain terms from the jth link. Formation of the recursive dynamic equations is developed below first for a terminal link and then for a non-terminal link.

4.1 Terminal body recursive dynamics

Equating the summation of forces and time derivative of linear momentum in the $j-1$ body frame for a terminal link j results in

$$\boldsymbol{R}_{j-1} + \mathbf{T}_I^{j-1}(\boldsymbol{F}_{\mathrm{D}j} + \boldsymbol{W}_j + \boldsymbol{F}_{\mathrm{A}}) = m_j \left(\mathbf{T}_{j-1}^{j}\right)^{\mathrm{T}} \boldsymbol{a}_j^{\mathrm{m}} \tag{20}$$

Summing moments about the connection joint c_{j-1} for the terminal link and equating to the time derivative of angular momentum in the j body frame yields

$$\begin{aligned} &\boldsymbol{r}_j^{\mathrm{m}} \times \mathbf{T}_I^{j}(\boldsymbol{F}_{\mathrm{D}j} + \boldsymbol{W}_j) + \boldsymbol{r}_j^{\mathrm{c}} \times \mathbf{T}_I^{j}\boldsymbol{F}_{\mathrm{A}} + \mathbf{T}_{j-1}^{j}\boldsymbol{L}_{j-1} \\ &\quad = (\mathbf{I}_j\boldsymbol{\alpha}_{j/I} + \boldsymbol{\omega}_{j/I} \times \mathbf{I}_j\boldsymbol{\omega}_{j/I}) + \boldsymbol{r}_j^{\mathrm{m}} \times m_j\boldsymbol{a}_j^{\mathrm{m}} \end{aligned} \tag{21}$$

The $\boldsymbol{i}$ component of both sides of the moment summation (21) reduce to zero due to each link being a body of revolution and the fact that the position vector from connection joint $j-1$ to the mass centre of the terminal link is defined such that it only has an $\boldsymbol{i}$ component. The remaining equations for the terminal link are assembled into a 5×1 force vector, $\boldsymbol{F}_j$, and arranged such that the first two equations represent the two non-zero components of the moment equation while the remaining three equations are components of the force equation (20). The force vector takes the form

$$\boldsymbol{F}_j = \mathbf{M}_j\dot{\boldsymbol{\nu}}_j + \boldsymbol{\Gamma}_T \tag{22}$$

where equation (15) is incorporated in to both equations (20) and (21) and

$$\boldsymbol{F}_j = \begin{Bmatrix} 0 \\ \boldsymbol{R}_{j-1} \end{Bmatrix}, \quad \mathbf{M}_j = \begin{bmatrix} \tilde{\mathbf{I}}_j - m_j\tilde{\mathbf{S}}_j^{\mathrm{m}}\tilde{\mathbf{S}}_j^{\mathrm{m}} & m_j\hat{\mathbf{S}}_j^{\mathrm{m}}\mathbf{T}_{\mathrm{j-1}}^{\mathrm{j}} \\ m_j\left(\mathbf{T}_{j-1}^{j}\right)^{\mathrm{T}}\left(\hat{\mathbf{S}}_j^{\mathrm{m}}\right)^{\mathrm{T}} & m_j\mathbf{E}_3 \end{bmatrix} \tag{23}$$

$$\tilde{\mathbf{I}}_j = \begin{bmatrix} I_{yy} & 0 \\ 0 & I_{zz} \end{bmatrix}, \quad \tilde{\mathbf{S}}_j^{\mathrm{m}} = \begin{bmatrix} 0 & -x_{\mathrm{m}j} \\ x_{\mathrm{m}j} & 0 \end{bmatrix},$$

$$\hat{\mathbf{S}}_j^{\mathrm{m}} = \begin{bmatrix} 0 & 0 & -x_{\mathrm{m}j} \\ 0 & x_{\mathrm{m}j} & 0 \end{bmatrix} \tag{24}$$

$$\boldsymbol{\Gamma}_T = \begin{bmatrix} -\hat{\mathbf{S}}_j^{\mathrm{m}}\mathbf{T}_I^{j}(\boldsymbol{F}_{\mathrm{D}j} + \boldsymbol{W}_j) - \hat{\mathbf{S}}_j^{\mathrm{c}}\mathbf{T}_I^{j}\boldsymbol{F}_{\mathrm{A}} - \hat{\mathbf{T}}_{j-1}^{j}\tilde{\boldsymbol{L}}_{j-1} \\ m_j\left(\mathbf{T}_{j-1}^{j}\right)^{\mathrm{T}}(\boldsymbol{\omega}_{j/I} \times \boldsymbol{\omega}_{j/I} \times \boldsymbol{r}_j^{\mathrm{m}}) \\ -\mathbf{T}_I^{j-1}(\boldsymbol{F}_{\mathrm{D}j} + \boldsymbol{W}_j + \boldsymbol{F}_{\mathrm{A}}) \end{bmatrix} \tag{25}$$

Note: due to the fact that the position vector from connection joint $j-1$ to the mass centre of the terminal link is defined such that it only has an $\boldsymbol{i}$ component, the links are bodies of revolution, and the spin rate in equation (4) is zero, the terms $\boldsymbol{r}_j^{\mathrm{m}} \times m_j(\boldsymbol{\omega}_{j/I} \times \boldsymbol{\omega}_{j/I} \times \boldsymbol{r}_j^{\mathrm{m}})$ and $\boldsymbol{\omega}_{j/I} \times \mathbf{I}_j\boldsymbol{\omega}_{j/I}$ from equation (21) vanish.

Earlier, the kinematic relationship for the acceleration vector, $\dot{\boldsymbol{\nu}}_j$, was defined in equation (17). Substituting equation (17) into equation (22) gives a relationship for the force vector, $\boldsymbol{F}_j$, in terms of the relative angular acceleration vector, $\dot{\boldsymbol{\omega}}_j$, expressed as

$$\boldsymbol{F}_j = \mathbf{M}_j(\mathbf{D}_j\dot{\boldsymbol{\nu}}_{j-1} + \mathbf{G}_j\dot{\boldsymbol{\omega}}_j + \boldsymbol{\Lambda}_j) + \boldsymbol{\Gamma}_T \tag{26}$$

Multiplying equation (26) by $\mathbf{G}_j^{\mathrm{T}}$ and noting that $\mathbf{G}_j^{\mathrm{T}}\boldsymbol{F}_j = 0$, $\dot{\boldsymbol{\omega}}_j$ for the terminal link takes the form

$$\dot{\boldsymbol{\omega}}_j = -(\mathbf{G}_j^{\mathrm{T}}\mathbf{M}_j\mathbf{G}_j)^{-1}\mathbf{G}_j^{\mathrm{T}}(\mathbf{M}_j\mathbf{D}_j\dot{\boldsymbol{\nu}}_{j-1} + \mathbf{M}_j\boldsymbol{\Lambda}_j + \boldsymbol{\Gamma}_T) \tag{27}$$

Substitution of the relative angular acceleration in equation (27) and the acceleration vector $\dot{\boldsymbol{\nu}}_j$ in equation (17) into the force vector in equation (22) results in a final expression for the terminal body's force vector expressed only using its forces and the parent body's joint accelerations which takes the form

$$\boldsymbol{F}_j = \hat{\mathbf{M}}_j\mathbf{D}_j\dot{\boldsymbol{\nu}}_{j-1} + \hat{\boldsymbol{\Gamma}}_j \tag{28}$$

where

$$\mathbf{K}_j = \mathbf{M}_j\mathbf{G}_j\left(\mathbf{G}_j^{\mathrm{T}}\mathbf{M}_j\mathbf{G}_j\right)^{-1} \tag{29}$$

$$\boldsymbol{\Gamma}_j^a = \boldsymbol{\Gamma}_T + \mathbf{M}_j\boldsymbol{\Lambda}_j \tag{30}$$

$$\hat{\boldsymbol{\Gamma}}_j = \boldsymbol{\Gamma}_j^a - \mathbf{K}_j\mathbf{G}_j^{\mathrm{T}}\boldsymbol{\Gamma}_j^a \tag{31}$$

$$\hat{\mathbf{M}}_j = \mathbf{M}_j - \mathbf{K}_j\mathbf{G}_j^{\mathrm{T}}\mathbf{M}_j \tag{32}$$

4.2 Non-terminal body recursive dynamics

The vector equations for the non-terminal links are formed in a similar fashion as to the terminal link. Forces are summed on each of these links while moments are summed about the c_{j-1} connection joint for each jth link in the tether. Again, the moment equations are expressed in the j body frame while the force equations are expressed in the $j-1$ body frame. By summing forces on these links, it is shown that

all non-terminal links have the equivalent recursive form

$$\boldsymbol{R}_{j-1} - \left(\mathbf{T}_{j-1}^{j}\right)^{\mathrm{T}} \boldsymbol{R}_j + \mathbf{T}_I^{j-1}(\boldsymbol{F}_{\mathrm{D}j} + \boldsymbol{W}_j) = m_j \left(\mathbf{T}_{j-1}^{j}\right)^{\mathrm{T}} \boldsymbol{a}_j^{\mathrm{m}} \tag{33}$$

The moment equation then takes the form

$$\begin{aligned} &\boldsymbol{r}_j^{\mathrm{m}} \times \mathbf{T}_I^{j}(\boldsymbol{F}_{\mathrm{D}j} + \boldsymbol{W}_j) - \boldsymbol{r}_j^{\mathrm{c}} \times \boldsymbol{R}_j + \mathbf{T}_{j-1}^{j} \boldsymbol{L}_{j-1} - \boldsymbol{L}_j \\ &\quad = (\mathbf{I}_j \boldsymbol{\alpha}_{j/I} + \boldsymbol{\omega}_{j/I} \times \mathbf{I}_j \boldsymbol{\omega}_{j/I}) + \boldsymbol{r}_j^{\mathrm{m}} \times m_j \boldsymbol{a}_j^{\mathrm{m}} \end{aligned} \tag{34}$$

The two expressions from equations (33) and (34) may now be assembled into matrix form in a similar fashion to that of the terminal link. The $\boldsymbol{i}$ component of the moment equation vanishes and the matrix form reduces to a 5×1 system. Non-terminal links all have the equivalent form

$$\boldsymbol{F}_j = \mathbf{M}_j \dot{\boldsymbol{\nu}}_j + \boldsymbol{\Gamma}_j + \mathbf{D}_{j+1}^{\mathrm{T}} \boldsymbol{F}_{j+1} \tag{35}$$

with

$$\boldsymbol{\Gamma}_j = \begin{bmatrix} -\hat{\mathbf{S}}_j^{\mathrm{m}} \mathbf{T}_I^{j}(\boldsymbol{F}_{\mathrm{D}j} + \boldsymbol{W}_j) - \hat{\mathbf{T}}_{j-1}^{j} \tilde{\boldsymbol{L}}_{j-1} + \tilde{\boldsymbol{L}}_j \\ m_j \left(\mathbf{T}_{j-1}^{j}\right)^{\mathrm{T}} (\boldsymbol{\omega}_{j/I} \times \boldsymbol{\omega}_{j/I} \times \boldsymbol{r}_j^{\mathrm{m}}) - \mathbf{T}_I^{j-1}(\boldsymbol{F}_{\mathrm{D}j} + \boldsymbol{W}_j) \end{bmatrix} \tag{36}$$

As with the terminal link, the terms $\boldsymbol{r}_j^{\mathrm{m}} \times m_j(\boldsymbol{\omega}_{j/I} \times \boldsymbol{\omega}_{j/I} \times \boldsymbol{r}_j^{\mathrm{m}})$ and $\boldsymbol{\omega}_{j/I} \times \mathbf{I}_j \boldsymbol{\omega}_{j/I}$ become zero. The force vector (35) for the jth body is coupled to the force vector from the previous link by the term $\mathbf{D}_{j+1}^{\mathrm{T}} \boldsymbol{F}_{j+1}$. It can be shown that the force vector for any non-terminal link can be written just as the terminal link (28) where it depends on its forces and the parent body's joint accelerations. Consider equation (35) for the terminal link's parent. Substitution of the terminal link force vector (28) into equation (35) results in

$$\boldsymbol{F}_j = \tilde{\mathbf{M}}_j \dot{\boldsymbol{\nu}}_j + \tilde{\boldsymbol{\Gamma}}_j \tag{37}$$

where

$$\tilde{\mathbf{M}}_j = \mathbf{M}_j + \mathbf{D}_{j+1}^{\mathrm{T}} \hat{\mathbf{M}}_{j+1} \mathbf{D}_{j+1} \tag{38}$$

$$\tilde{\boldsymbol{\Gamma}}_j = \boldsymbol{\Gamma}_j + \mathbf{D}_{j+1}^{\mathrm{T}} \hat{\boldsymbol{\Gamma}}_{j+1} \tag{39}$$

Similar to the terminal link, substitution of equation (17) into equation (37) gives a relationship for the force vector, $\boldsymbol{F}_j$, in terms of the relative angular acceleration vector, $\dot{\boldsymbol{\omega}}_j$. Multiplying the result by $\mathbf{G}_j^{\mathrm{T}}$ and noting that $\mathbf{G}_j^{\mathrm{T}} \boldsymbol{F}_j = 0$, $\dot{\boldsymbol{\omega}}_j$ for the terminal link takes the form

$$\dot{\boldsymbol{\omega}}_j = -(\mathbf{G}_j^{\mathrm{T}} \tilde{\mathbf{M}}_j \mathbf{G}_j)^{-1} \mathbf{G}_j^{\mathrm{T}} (\tilde{\mathbf{M}}_j \mathbf{D}_j \dot{\boldsymbol{\nu}}_{j-1} + \boldsymbol{\Gamma}_j^{a}) \tag{40}$$

where

$$\boldsymbol{\Gamma}_j^{a} = \tilde{\boldsymbol{\Gamma}}_j + \tilde{\mathbf{M}}_j \boldsymbol{\Lambda}_j \tag{41}$$

Finally, equations (17) and (40) can be combined with equation (37) such that the non-terminal link force vector takes the form

$$\boldsymbol{F}_j = \hat{\mathbf{M}}_j \mathbf{D}_j \dot{\boldsymbol{\nu}}_{j-1} + \hat{\boldsymbol{\Gamma}}_j \tag{42}$$

with

$$\mathbf{K}_j = \tilde{\mathbf{M}}_j \mathbf{G}_j \left(\mathbf{G}_j^{\mathrm{T}} \tilde{\mathbf{M}}_j \mathbf{G}_j\right)^{-1} \tag{43}$$

$$\hat{\boldsymbol{\Gamma}}_j = \boldsymbol{\Gamma}_j + \tilde{\mathbf{M}}_j \boldsymbol{\Lambda}_j - \mathbf{K}_j \mathbf{G}_j^{\mathrm{T}} \boldsymbol{\Gamma}_j^{a} \tag{44}$$

$$\hat{\mathbf{M}}_j = \tilde{\mathbf{M}}_j - \mathbf{K}_j \mathbf{G}_j^{\mathrm{T}} \tilde{\mathbf{M}}_j \tag{45}$$

It follows that since force vector for the parent of the terminal link also takes the recursive form in equation (42), the process can be repeated for each subsequent non-terminal link with the same force vector expression resulting.

4.3 Number of computations

The recursive solution begins with a backward pass through the tether system starting at the terminal link. At the terminal link ($j = N$) the force vector, $\boldsymbol{F}_j$, in equations (22) and (28) can be formed. Formation of force vectors for all non-terminal links then follows for $j = N - 1$ to 1 using equations (37) and (42). Upon reaching the root link ($j = 1$), the acceleration vector $\dot{\boldsymbol{\nu}}_1$ in equation (37) becomes solvable. Since the root link is attached to the ground, $\boldsymbol{a}_0^{\mathrm{c}}$ is zero and the solution to $\tilde{\boldsymbol{\alpha}}_{1/I}$ only requires the inversion of a 2×2 matrix. Therefore, the solution to $\dot{\boldsymbol{\nu}}_1$ is found at the end of the 'backwards pass'. Once the acceleration vector, $\dot{\boldsymbol{\nu}}_1$, for the root link is known, a forward pass is used to find the angular acceleration vector, $\dot{\boldsymbol{\omega}}_j$, and the acceleration vector, $\dot{\boldsymbol{\nu}}_j$, using equations (40) and (17) for $j = 2$ to $N - 1$ then equations (27) and (17) for $j = N$. Completion of the 'forward pass' results in the solution to the N angular accelerations, $\tilde{\boldsymbol{\alpha}}_{j/I}$, for $j = 1$ to N required for numerical integration.

In order to evaluate the proposed method's efficiency, the number of floating point operations (FLOPs), including addition, subtraction, multiplication, and division, is evaluated starting at the beginning of the backward pass where the link position, angular velocities, geometry, and link inertias are already known. The sparse structure of matrices such as $\mathbf{G}_j$ and $\mathbf{D}_j$ in equation (18) along with equations (19) and (24) are considered in evaluation of the number of computations. The computations of the proposed method excluding spin dynamics will be compared to what is referred to as the general tether model which includes spin dynamics. The algorithm for the general model proceeds just as the proposed method; however, each link has three DOFs resulting in the angular velocity of jth body (equation (4)) having three components resulting in many of the vectors and matrices becoming larger by one dimension.

Computations during the backward pass can be divided into three categories: non-terminal links, terminal link, and the root link. Computations required for the terminal links in equations (23) to (32) include $\mathbf{M}_j, \mathbf{K}_j, \boldsymbol{\Gamma}_T, \boldsymbol{\Lambda}_j, \boldsymbol{\Gamma}_j^a, \hat{\boldsymbol{\Gamma}}_j, \hat{\mathbf{M}}_j$ resulting in 308 FLOPs. Non-terminal links require evaluation of similar parameters in equations (38) to (45) requiring 742 FLOPs. Completion of the backward pass requires only calculation of $\mathbf{M}_j, \tilde{\mathbf{M}}_j, \tilde{\boldsymbol{\Gamma}}_j$ for the root link resulting in only 373 FLOPs. Combining all three categories results in $742(N-2)+681$ FLOPs for the backward pass of the proposed method where spin dynamics are neglected. In comparison, the backward pass for the general recursive algorithm where spin dynamics are included results in $1463(N-2)+1553$ FLOPs.

The forward pass is initiated by first finding $\dot{\boldsymbol{v}}_1$ of the root link from equation (37), requiring 13 FLOPs. The remaining non-terminal and terminal link dynamics, $\dot{\boldsymbol{\omega}}_j$ and $\dot{\boldsymbol{v}}_j$, are found for $j=1$ to N using equations (40) and (17) requiring 92 FLOPs for each link noting that many parameters were previously found in the backward pass. The complete forward pass then requires $92(N-1)+13$ FLOPs for the proposed method compared to $203(N-1)+56$ for the general recursive method including spin dynamics. Combining the backward and forward passes results in a total of $834N-786$ FLOPs for the proposed method compared to $1666N-1520$ for the general recursive method, demonstrating that the proposed recursive dynamic algorithm for a tether requires approximately half the computations of the general recursive dynamic algorithm.

Computational results above can be compared to other recursive algorithms for a serial chain of N rigid bodies with the evaluation of some well-established recursive methods provided and discussed in references [**16**] and [**18**]. Both references [**16**] and [**18**] evaluate the simplified case where each body is attached by a revolute joint often used in robotic manipulators, resulting in each body possessing only a single DOF. Assessments of computations required for such a case are similar, with reference [**16**] concluding $703 \times \mathrm{N} + 370$ FLOPs are required, while Stelzle *et al.* [**18**] conclude $621 \times \mathrm{N} - 590$ FLOPs are required. Differences between the two are because reference [**18**] reduces computations by calculating some auxiliary matrices and judiciously using reference frames. Comparison of all three methods: the general model using three DOFs, the proposed method excluding spin dynamics, and simple chain using single DOF revolute joints, shows that the proposed method results in half the computations of the general chain, while requiring only slightly more computations than the simpler revolute joint chain. However, it is noted that in reference [**18**] the method is general in the sense of not applying any reduction to the 6×6 matrices, making direct comparisons between both methods not so obvious.

5 EXAMPLE

Once the general case of the recursive formulation for a multi-body system is complete, a specific tether may be modelled which consists of N rigid links, that when connected by the spherical joints gives the tether a total length of l_T and an overall mass of m_T. The mass and dimensions of the joints connecting the links are small in comparison to those of the individual tether links; thus, they are ignored. The links have identical geometry and are assumed to be solid, slender cylindrical rods of lengths $l_j = l_T/N$, and equivalent masses of $m_j = m_T/N$. In addition, the defined geometry yields a 2×2 inertia matrix for each jth link expressed as

$$\tilde{\mathbf{I}}_j = \begin{bmatrix} \dfrac{m_j l_j^2}{12} & 0 \\ 0 & \dfrac{m_j l_j^2}{12} \end{bmatrix} \tag{46}$$

Also as previously noted, the tether is attached to the ground by the root link ($j=1$) at joint c_0 and with the load, $\boldsymbol{F}_A$, applied to its terminal link.

5.1 Forces and moments

Forces present on each link consist of reaction forces that exist at each joint, the weight of the link, and the aerodynamic drag which is assumed to be an applied load that is a function of the link geometry and attached to the mass centre of the link. Each link is a cylindrical; thus, from reference [**19**] the aerodynamic drag is approximated as

$$\boldsymbol{F}_{Dj} = -\frac{1}{2} C_D \rho_A s_j |\boldsymbol{V}_j| \boldsymbol{V}_j \tag{47}$$

where the drag coefficient is $C_D = 1.17$, ρ_A is the air density, $\boldsymbol{V}_j$ is the mass centre velocity, and s_j is the link's frontal area, all for the jth link.

In addition to the aerodynamic drag on each link, a damping moment is assumed to exist in each joint. Joint damping is modelled as viscous damping, proportional to the bending rate between two successive links. Geometrically, this can be viewed as the relative angular velocity of two links only in the plane they form, that is damping comes only from the relative link bending and not the twist. The relative bending rate between two links is found by taking the difference between the components of each link's angular velocity which are normal to both links. A tether is assumed to have a total damping coefficient C_S. An individual link damping coefficient, C_{Sj}, is scaled by mass and length according to

$$C_{Sj} = C_S m_j l_j^{1.5} \tag{48}$$

5.2 Lumped mass comparison

An example tether was defined with overall length of $l_T = 10$ m, a diameter of $d = 1.5875$ mm made of nine strands of stainless steel, total mass of 0.16 kg, and C_S of 0.13 $\sqrt{m/s^2}$. Simulations of the proposed rigid-body model and a lumped mass bead model with masses connected by spring and dampers in parallel were completed for comparisons. Both models used 32 elements with simulations initiated from rest, 5° away from vertical, and no applied force. The bead model had individual element stiffness of 256 N/m resulting is a static strain of approximately one percent due to its own weight. The bead damping coefficients were selected as 0.018 kg/s so that both the tether and bead models had similar responses. The non-linear differential equations were numerically integrated using a fourth-order Runge–Kutta algorithm with 0.005 s time step.

Comparisons of the link and bead models are shown in Figs 5 to 8, with Figs 5 and 6 comparing the position and velocities of the tether midpoint, while Figs 7 and 8 compare the position and velocities for the tether endpoint. It can be seen in both Figs 5 and 7 that while the bead model begins to exhibit some higher-frequency velocities the overall pendulum motion of the tether matches well between the link and bead model. However, Figs 6 and 8 demonstrate that both axial position and velocity of the bead model exhibit high-frequency motion not seen in the rigid link model. It is important to note that some axial vibration can be alleviated by increasing the bead model damping; however, due to coupling, the pendulum motion in Figs 5 and 7 also decays more rapidly. This is in contrast to the rigid link model where joint damping contributes mainly

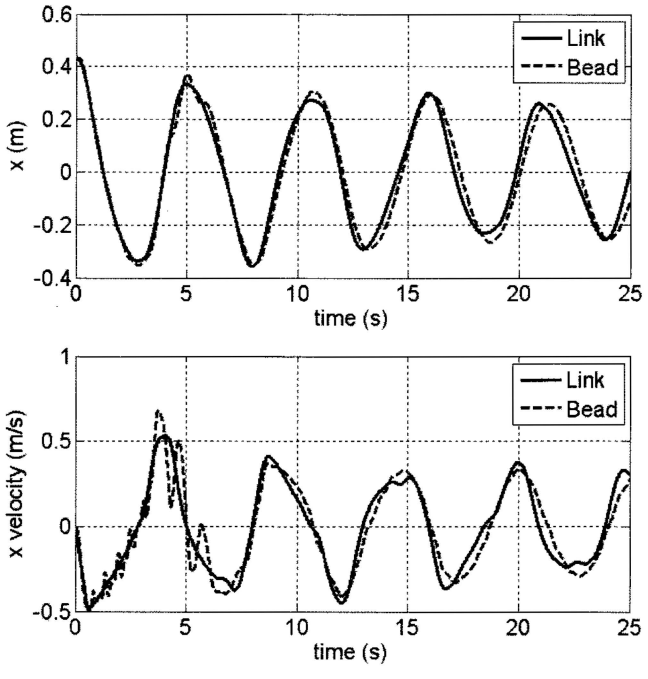

Fig. 5 X position and velocity at the middle of a tether

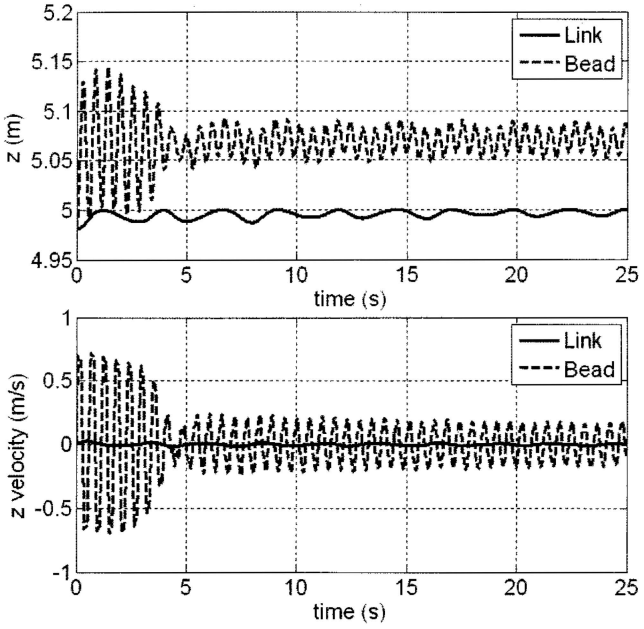

Fig. 6 Z position and velocity at the middle of a tether

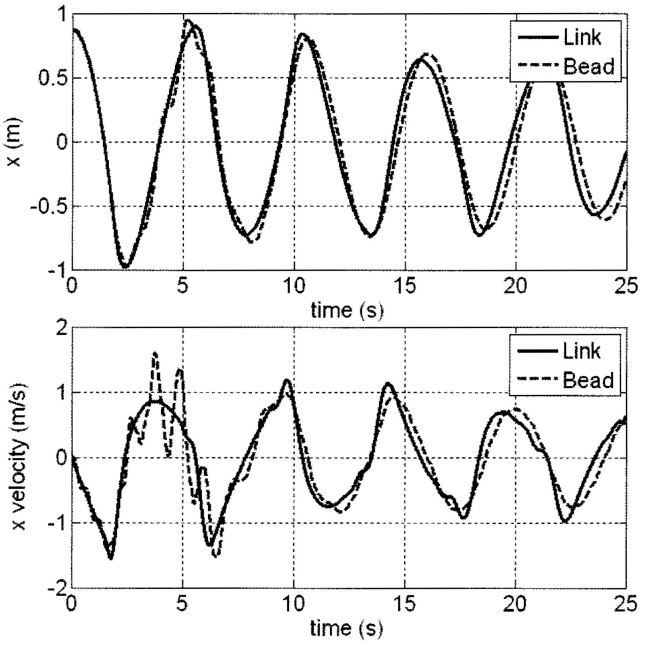

Fig. 7 X position and velocity at the end of a tether

to the relative motion of links with respect to each other, while the aerodynamic drag is the most significant parameter determining the overall decay of the rigid-body pendulum motion. Figures 6 and 8 show the effect of static stiffness on the midpoint and endpoint deflection.

5.3 Tether discretization

Simulations were completed using the tether discussed in the previous section using 8, 16, 32, 64, and 128 links with an applied tip load. The load at the

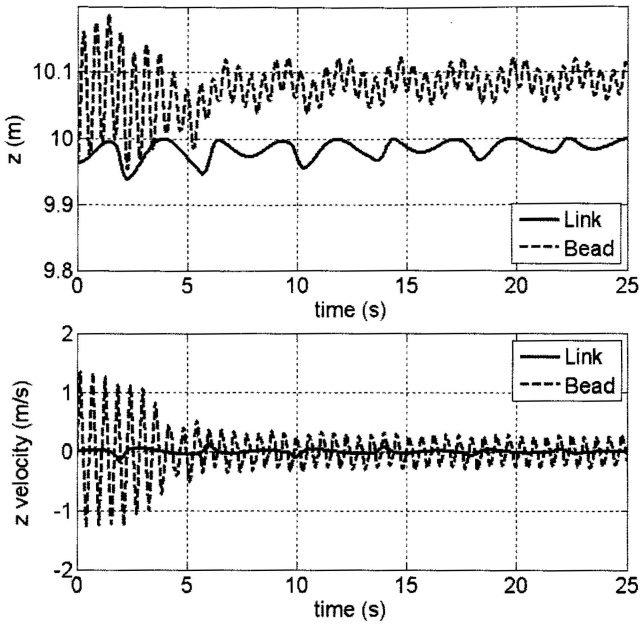

Fig. 8 Z position and velocity at the end of a tether

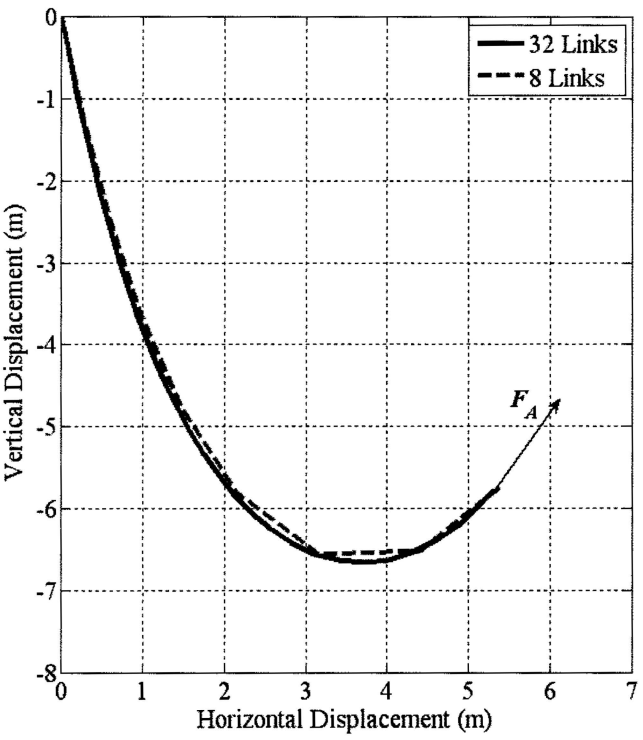

Fig. 9 Steady-state deformation for eight- and 32-link tethers

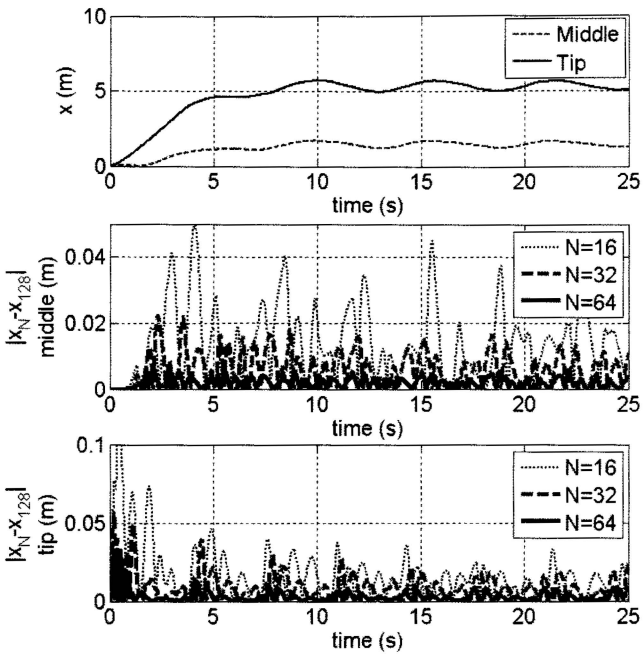

Fig. 10 X position of a 128-link tether midpoint and endpoint compared with 16-, 32-, and 64-link tethers

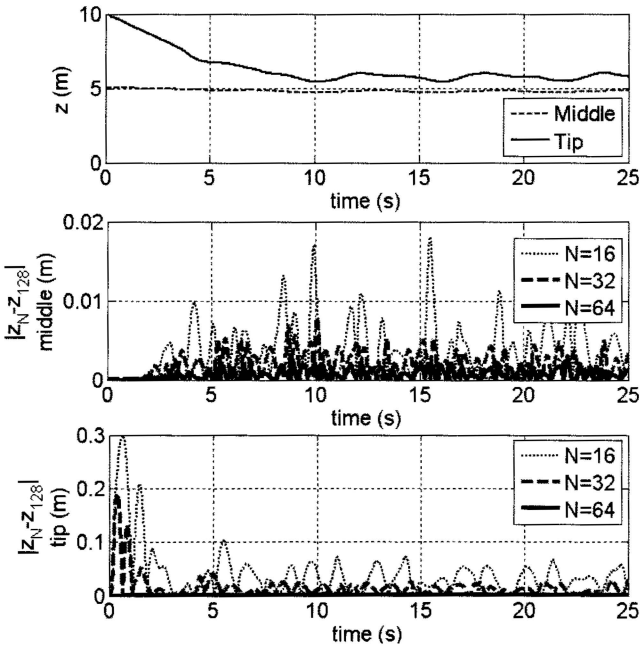

Fig. 11 Z position of a 128-link tether midpoint and endpoint compared with 16, 32, and 64-link tethers

terminal link had a magnitude increasing from 0 per cent to 25 per cent of the overall weight of the tether over 10 s and was applied at an angle of positive 50° with respect to the horizontal in the vertical plane defined by the $\boldsymbol{i}_I$ and $\boldsymbol{k}_I$ axes. Simulations were initiated with the tether hanging down vertically at rest. An advantage of increasing the number of links is the model has a better-defined geometry that more accurately models the deformation of the tether. The model consisting of 32 links exhibited an appropriate curvature and deformation once the steady-state conditions were attained under the applied load, $\boldsymbol{F}_A$. Figure 9 is an illustration of the eight-link and the 32-link tether once the steady state of the simulation was achieved.

Another important aspect of the tether models is the dynamic response of the tether to the applied loading. Figures 10 to 12 show the X position, Z position, and

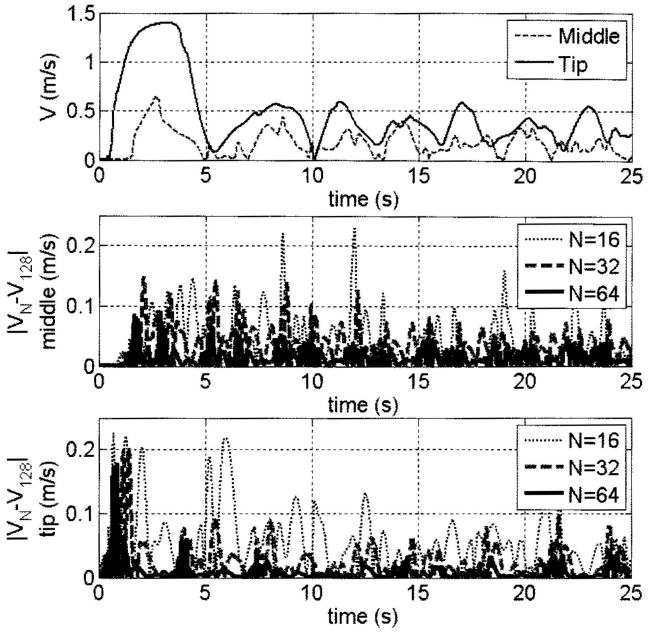

Fig. 12 Total velocity of a 128-link tether midpoint and endpoint compared with 16-, 32-, and 64-link tethers

total velocity time histories for both the tether midpoint and endpoint using 16, 32, 64, and 128 links. In each figure, the top line is the 128 link tether while differences in position and velocities between the 16, 32, and 64 link tethers are shown below for both the midpoint and endpoint. It can be seen from the three figures that as the number of links are increased the position and velocity trajectories converge, with the difference between the 64 and 128 link tether being small.

6 CONCLUSION

A computationally efficient discrete model for low-strain tethers used in many engineering applications was developed without the use of elastic elements. The model was based on a joint-coordinate formulation resulting in a set of unconstrained differential equations. Each link is treated as a body of revolution and it is assumed that tether spin is negligible to the dynamics resulting in each link having only two DOFs. A recursive algorithm was then developed where it was shown that the proposed method requires approximately half the computations as general recursive rigid-body methods. Through a comparison of the proposed method and a bead model, it was shown that the increased complexity of using rigid bodies over lumped point mass models with stiff elastic elements was justified by the elimination of high-frequency axial vibrations. The absence of high-frequency axial vibration allows larger integration time steps, further improving computation speeds. The result is a computationally efficient model that can accurately represent a low-strain tether used in many engineering applications without the need to add stiff elastic elements.

REFERENCES

1 **Aglietti, G.** Dynamic response of a high-altitude tethered balloon system. *J. Aircr.*, 2009, **46**(6), 2032–2040.
2 **Bono, C. G.** and **Perkins, N. C.** Physical and numerical modeling of the dynamic behavior of a fly line. *J. Sound Vibr.*, 2002, **255**(3), 555–577.
3 **Bono, C. G.** and **Perkins, N. C.** Numerical model for the dynamics of a coupled fly line/fly rod system and experimental validation. *J. Sound Vibr.*, 2004, **272**(3), 773–791.
4 **Williams, P.** and **Tivailo, P.** Dynamics of circularly towed cable systems, part 1: optimal configurations and their stability. *J. Guidance Control Dyn.*, 2007, **30**(3), 753–765.
5 **Kamman, J.** and **Huston, R.** Modeling of variable length towed and tethered cable systems. *J. Guidance Control Dyn.*, 1999, **20**(4), 602–608.
6 **Kyle, J.** and **Costello, M.** Comparison of measured and simulated motion of a scaled dragline excavation system. *Math. Compute. Model.*, 2006, **44**(4), 816–833.
7 **Frost, G.** and **Costello, M.** Improved deployment characteristics of a tether-connected munition system. *J. Guidance Control Dyn.*, 2001, **24**(3), 547–554.
8 **Bauchau, O. A., Bottasso, C. L.,** and **Nikishkov, Y. G.** Modeling rotorcraft dynamics with finite element multibody procedures. *Math. Comput. Model.*, 2001, **33**, 1113–1137.
9 **Bauchau, O. A.** and **Rodriguez, J.** Formulation of modal based elements in nonlinear, flexible multibody dynamics. *J. Multiscale Comput. Eng.*, 2003, **1**(2&3), 161–180.
10 **Orlandea, N. V.** From Newtonian dynamics to sparse Tableaux formulation and multi-body dynamics. *Proc. IMechE, Part K: Multi-body Dynamics*, 2008, **222**(4), 301–314. DOI: 10.1243/14644193JMBD153.
11 **Nikravesh, N. V.** Newtonian-based methodologies in multi-body dynamics. *Proc. IMechE, Part K: Multi-body Dynamics*, 2008, **222**(4), 277–288. DOI: 10.1243/14644193JMBD152.
12 **Jerkovsky, W.** The structure of multibody dynamic equations. *J. Guidance Control*, 1978, **1**(3), 173–182.
13 **Kane, T., Linkins, P.,** and **Levinson, D.** *Spacecraft dynamics*, 1983 (McGraw-Hill, New York).
14 **Hollerbach, J.** A recursive lagrangian formulation of manipulator dynamics and a comparative study of dynamic formulation complexity. *IEEE Trans. Syst. Man Cybern.*, 1980, **10**(11), 730–736.
15 **Schielen, W.** Computational dynamics: theory and application of multibody systems. *Eur. J. Mech. A/Solids*, 2006, **25**, 566–594.
16 **Tong, M.** Efficient treatment of gyroscopic bodies in the recursive solution of multibody dynamics equations. *J. Comput. Nonlinear Dyn.*, 2008, **3**(4), 041006-1–041006-6.
17 **Kuipers, J.** *Quaternions and rotation sequences*, 1999, pp. 103–136 (Princeton University Press, New Jersey).
18 **Stelzle, W., Kecskeméthy, A.,** and **Hiller, M.** A comparative study of recursive methods. *Arch. Appl. Mech.*, 1995, **66**, 9–19.

19 White, F. M. *Fluid mechanics*, 2nd Edition, 1986 (McGraw-Hill, New York).

APPENDIX

Notation

$\boldsymbol{a}_j^{\mathrm{c}}$	acceleration of the jth connection joint with respect to the inertial frame
$\boldsymbol{a}_j^{\mathrm{m}}$	acceleration of mass centre of the jth link with respect to the inertial frame
b_j	jth link of the tether (ground link $j = 0$, root link $j = 1$, parent body $j = j\mathrm{p}$)
c_j	jth connection joint (ground connection joint $j = 0$)
C_{D}	drag coefficient
C_S	tether damping coefficient
C_{Sj}	damping coefficient of the jth link
d	diameter of the tether
$\mathbf{E}_n$	$n \times n$ identity matrix
$\boldsymbol{F}_{\mathrm{A}}$	constant applied load attached to the terminal link of the tether
$\boldsymbol{F}_{\mathrm{D}j}$	drag force for the jth link
$\boldsymbol{F}_j$	5×1 force vector for the jth link
I	inertial reference frame defined by a triad of unit vectors $\boldsymbol{i}_I, \boldsymbol{j}_I, \boldsymbol{k}_I$
$\mathbf{I}_j$	inertia matrix of the jth body
$\tilde{\mathbf{I}}_j$	2×2 inertia matrix consisting of I_{yy} and I_{zz}
I_{nn}	mass moment of inertia about i, j, k body axes with $n = x, y, z$, respectively
l_j	length of the individual jth link
l_T	overall tether length
$\boldsymbol{L}_j$	moment in jth connection joint acting on the $j + 1$ link and the jth link, respectively
$\tilde{\boldsymbol{L}}_j$	2×1 moment vector consisting of $\boldsymbol{j}$ and $\boldsymbol{k}$ components of $\boldsymbol{L}_j$
L_{nj}	nth component of $\boldsymbol{L}_j$ with $n = x, y, z$, respectively
m_j	mass of link j
m_T	total mass of the tether
N	total number of tether links
p_j, q_j, r_j	angular velocity components of the jth link
$q_{0j}, q_{1j}, q_{2j}, q_{3j}$	quaternion parameters for the jth link
$\boldsymbol{r}_j^{\mathrm{m}}, \boldsymbol{r}_j^{\mathrm{c}}$	vector from connection $j - 1$ to mass centre j and connection j
$\boldsymbol{R}_j$	reaction in jth connection joint acting on the $j + 1$ link and the jth link, respectively
s_j	frontal area of the jth link
$\hat{\mathbf{S}}_j^{\mathrm{c}}$	2×3 submatrix of skew symmetric cross-product operator for position vector for $\boldsymbol{r}_j^{\mathrm{c}}$
$\hat{\mathbf{S}}_j^{\mathrm{m}}$	2×3 submatrix of skew symmetric cross-product operator for position vector for $\boldsymbol{r}_j^{\mathrm{m}}$
$\tilde{\mathbf{S}}_j^{\mathrm{m}}$	2×2 submatrix for skew symmetric cross-product operator for position vector $\boldsymbol{r}_j^{\mathrm{m}}$
$\mathbf{T}_I^j$	transformation from inertial to the jth body frame
$\mathbf{T}_{j-1}^j$	transformation from the $j - 1$ body frame to the jth body frame
$\hat{\mathbf{T}}_{j-1}^j$	2×2 submatrix of the second and third columns of the second and third rows of $\mathbf{T}_{j-1}^j$
$\tilde{\mathbf{T}}_{j-1}^j$	1×2 submatrix of the second and third elements of the first row of $\mathbf{T}_{j-1}^j$
$\dot{\boldsymbol{v}}_j$	5×1 acceleration vector consisting components of $\tilde{\boldsymbol{\alpha}}_{j/I}$ and $\boldsymbol{a}_{j-1}^{\mathrm{c}}$, respectively
$\boldsymbol{V}_j$	mass centre velocity of the jth link
$\boldsymbol{W}_j$	weight of the jth link
x_{cj}, x_{mj}	length from $j - 1$ connection to the jth connection and mass centre
$\boldsymbol{\alpha}_{j/I}$	angular acceleration vector of the jth link with respect to the inertial frame
$\tilde{\boldsymbol{\alpha}}_{j/I}$	2×1 angular acceleration vector consisting of $\boldsymbol{j}$ and $\boldsymbol{k}$ components of $\boldsymbol{\alpha}_{j/I}$
$\rho_{\mathrm{A}}, \rho_S$	air and tether densitiy
$\varphi_j, \theta_j, \psi_j$	jth link Euler angles
$\dot{\boldsymbol{\omega}}_j$	2×1 angular acceleration vector consisting of the j and k components of $\dot{\boldsymbol{\omega}}_{j/j-1}$
$\boldsymbol{\omega}_{j/I}$	angular velocity vector of the jth link with respect to the inertial frame
$\tilde{\boldsymbol{\omega}}_{j/I}$	2×1 angular velocity vector consisting of j and k components of $\boldsymbol{\omega}_{j/I}$
$\boldsymbol{\omega}_{j/j-1}$	relative angular velocity of the jth link with respect to the $j - 1$ link
ω_{nj}	nth component of $\boldsymbol{\omega}_{j/j-1}$ with $n = x, y, z$, respectively